

Data decoding of integer orbital angular momentum beams based in straight edge diffraction nanometric film

Jesús H. Mendoza-Castro^a, Carlos Fernando Díaz^a, Cristian Hernando Acevedo^a, Yezid Torres^b & Jaime Guillermo Barrero^c

^a GOTS, Universidad Industrial de Santander, Bucaramanga, Colombia. nachomendozac@hotmail.com, marck177@hotmail.com, crstncvd8@gmail.com

^b Escuela de Física, GOTS, Universidad Industrial de Santander, Bucaramanga, Colombia. ytorres@uis.edu.co

^c E3T, Universidad Industrial de Santander, Colombia. jbarrero@uis.edu.co

Received: August 8th, 2018. Received in revised form: March 1st, 2019. Accepted: March 27th, 2019.

Abstract

The orbital angular momentum revolutionized optical communications, since an OAM beam of light does not need to be interrupted for the transfer of data, provides immunity to electromagnetic interference, allows increase bandwidth, rate and transmission capacity information. Supported by the ability to encode information on OAM modes of light, methods and developments associated with the formulation and implementation of a data decoding architecture are shown, which uses spatial filters at nanoscale order. An improvement to techniques for detecting the topological charge of an OAM beam is introduced. Here is reduced to the diffraction of OAM beam by a straight edge and a triangular equilateral aperture analysis; due that the use of additional optics is suppressed which would be necessary for other techniques and decreases the cost of implementation. For this purpose, physics theory of OAM beams, arguments for selecting and design components of the decoder are presented, as well as experimental details, discussions and results, showing the feasibility of the proposed method for decoding information.

Keywords: orbital angular momentum; thin films; encoding; decoding; topological charge; optical communications.

Decodificación de datos de un haz láser con momento angular orbital entero basada en la difracción por el borde recto de una película nanométrica

Resumen

El momento angular orbital ha revolucionado la visión sobre las comunicaciones ópticas, ya que un haz de luz MAO no necesita interrumpirse para el traspaso de datos, confiere inmunidad a la interferencia electromagnética, permite un aumento en el ancho de banda, la tasa de transmisión y la capacidad de información. Sustentados en la posibilidad de codificar información en los diferentes modos del haz de luz, se presentan métodos y desarrollos asociados con la formulación e implementación de una arquitectura de decodificación, usando filtros espaciales de orden nanométrico. Se introduce una mejora a las técnicas de detección de la carga topológica de un haz MAO. Aquí, se reduce al análisis de la difracción por un borde recto y una abertura triangular equilátera. Además, se suprime el uso de óptica adicional necesaria en otras técnicas y reduce el costo de implementación. Con este propósito, teoría física de haces MAO, argumentos para la selección y diseño de componentes del decodificador, junto con detalles experimentales, muestran la viabilidad del método propuesto para decodificar información.

Palabras clave: momento angular orbital; películas delgadas; codificación; decodificación; carga topológica; comunicaciones ópticas.

1. Introduction

Throughout history, the development of the conception about the Physical world and its interaction with the

fundamental forces has given more relevance to light as one of the most important electromagnetic phenomena in the development of life, and, as a fundamental basis for many practical solutions that make our existence easier today.

How to cite: Mendoza-Castro, J.H., Díaz, C.F., Acevedo, C.H., Torres Y. and Barrero J.G., Data decoding of integer orbital angular momentum beams based in straight edge diffraction nanometric film. DYNA, 86(209), pp. 170-179, April - June, 2019.

Because of this, applications with the greatest impact within the four major areas of influence of optics (Instrumentation, Metrology, Communications, Border Optics), such as the industrial uses in medicine, biology, communications, environmental monitoring, among others, have promoted this topic. [1]. These developments have been based on the study of the behavior of some properties of light such as the intensity of data transmission or illumination, analysis of spectral content, associated with colors for the construction of images, Identification of compounds, etc., just to mention some applications [2]. The Spin Angular Momentum and the Orbital Angular Momentum characteristics of light have been recently described [3]; the latter with great potential to generate and to improve existing engineering applications within the communications networks, as it is described in the article from BBC News which highlights this new technology as very promising. [4]

The Orbital Angular Momentum OAM, has revolutionized many fields; it has especially transformed the vision on Optical Communications [5]. Currently sending data through an optical fiber uses a coding principle where bit 1 is associated to a light pulse, and in its absence bit 0 [7]. These features are surpassed by Orbital Angular Momentum, due to its lack of need to interrupt the beam for data transfer, providing immunity to electromagnetic interference, increasing bandwidth, transmission rate and channel capacity, thus making the communication process more efficient [6]. For these reasons, methods have currently been developed which allow a deep study of the applicability of OAM. Within these methods, techniques have been produced for generation and detection, with experimental procedures, such as: digital image processing [7], Holographic diffraction [5] and Interferometry [8] among others. Methods and developments associated with the construction and implementation of a data decoding architecture are shown. They use spatial filters at nanoscale order. For this purpose, physics theory of OAM beams is presented. The arguments for selecting and design components of the decoder, as well as experimental details, discussions and results, showing the feasibility of the proposed method for decoding information.

2. Theoretical Formulation

Consider a Bessel-Gauss beam with an integer topological charge m as an incident beam, whose electromagnetic field amplitude is given by [8,9]:

$$U(\rho, \theta, z_0) = c_0 e^{-\frac{\rho^2}{2w^2(z_0)}} e^{im\theta} \rho \left[I_{\left(\frac{m-1}{2}\right)} \left(\frac{\rho^2}{2w^2(z_0)} \right) - I_{\left(\frac{m+1}{2}\right)} \left(\frac{\rho^2}{2w^2(z_0)} \right) \right] \quad (1)$$

Where $c_0 = t \frac{\sqrt{\pi}}{2w_0} e^{i\frac{z}{z_r}} e^{i\frac{3\pi}{2}m} e^{ikz_0}$ is a complex constant, $w(z_0)$ the radius of the beam at the aperture plane, $R(z) = z \left[1 + \left(\frac{z_r}{z} \right)^2 \right]$ the radius of the wave front, $z_r = \frac{kw_0^2}{2}$ Rayleigh's range, w_0 is the beam waist, k is the wave number of monochrome OAM beam, and $I\left(m \pm \frac{1}{2}\right)$ are the

modified Bessel's functions. The term $e^{im\theta}$ expresses the OAM's phase, where the value of m indicates the number of rotations of the wave front on the propagation axis, which is called the topological charge.

As Fig. 1 shows, the phase representation is between -2π and 4π , for a range of 6π , equivalent to three rotations of the wavefront. The range display is possible thanks to the mapping of phase discontinuities mathematically limited to the interval $[-\pi, \pi]$.

Eq. (1) describes the field distribution at a distance $z = z_0$. At this z -position an equilateral triangular aperture is located. If it is taken into account that the transmittance function associated corresponds to the unit value at its interior and zero outside, it is easy to calculate its diffraction pattern far field, as shown in the Fig. 2.

The triangular aperture provides a simple and easy method for determining the magnitude and sign of the topological charge of the OAM beam. The number of external spots or spots along one of its sides minus one corresponds to the topological charge of the optical vortex [10]. When the OAM beam has an opposite topological charge, the triangular diffraction pattern far field, is rotated 180 degrees compared to original one [11].

In quantum mechanics, Born's rule predicts that quantum interference, for instance in a double-slit or Young's diffraction experiment, occurs through disjoint pairs of paths. A generalized version could allow multiple paths of interference. Sinha et al. performed a three-slit experiment, demonstrating the consistency of the postulate in both, semi classical and quantum regimes [12].

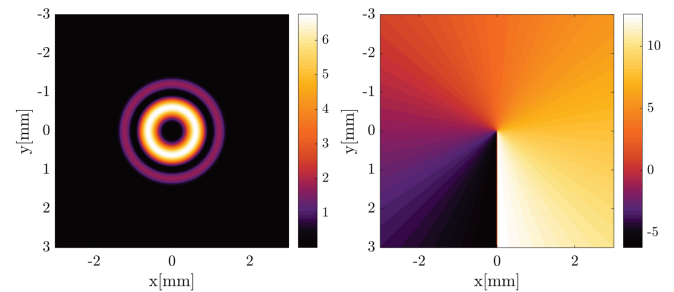


Figure 1. Magnitude (normalized energy) and phase (unwrapped) of a Bessel - Gauss beam, with topological charge $m = 3$. Source: The Authors.

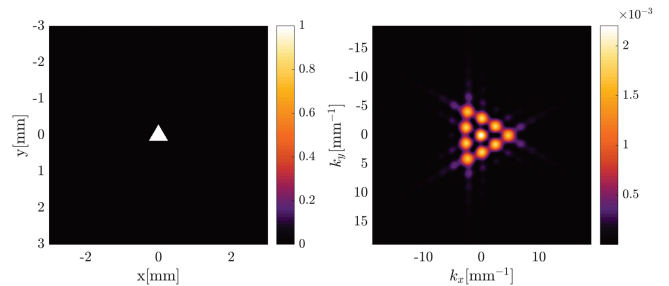


Figure 2. Diffraction pattern resulting from diffraction by numerical simulation of an OAM beam with TC, $m = 3$, through an equilateral triangular aperture. Source: The Authors.

Under Born rule, the diffraction pattern by the triangular equilateral aperture, viewed as a combination of slits, can be reconstructed from the interaction between the multiple pairs of disjoint slits that may be contained within the triangular slit.

Sorkin [13], proposes a series of configurations of symmetrical functions, which generalize the terms of interference. Considering that A, B, C are mutually disjoint sets, meaning the intersection between them is empty.

$$I_3(A, B, C) \equiv |A \cup B \cup C| - |A \cup B| - |B \cup C| - |A \cup C| + |A| + |B| + |C| \quad (2)$$

In eq. (2) the interference is described for three sets, which are intrinsically related to double and single sets, where A, B, C represent the set of points, which form the apertures thus labeled (See Fig. 3). $I_3(A, B, C)$ is the conjoint probability and, $|A|, |B|, |C|$, the probabilities that present a quantum measure of sets A, B, C or its appropriate combination, respectively. \cup represents the union of the disjoint sets.

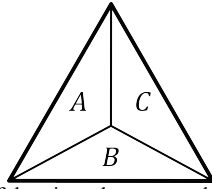


Figure 3. Composition of the triangular aperture by three disjoint slits. Source: The Authors.

Sinha et al.[12], make an interpretation of the Born rule for individual photons from wave functions that define the probability density to find a particle in a position \vec{r} in a time t . In the double slit diffraction experiment (A, B) you can see that:

$$P_{AB}(\vec{r}) = |\psi_A(\vec{r}) + \psi_B(\vec{r})|^2 \quad (3)$$

meaning,

$$P_{AB}(\vec{r}) = |\psi_A|^2 + |\psi_B|^2 + \psi_B^* \psi_A + \psi_A^* \psi_B \quad (4)$$

$$P_{AB}(\vec{r}) = P_A + P_B + I_{AB} \quad (5)$$

Where P_i Corresponds to the probability that a photon, through the slit i ($i = A, B$) y ψ_A^* represents the conjugate complex. Hence this results in the second-order interference term:

$$I_{AB} = P_{AB} - P_A - P_B \quad (6)$$

Considering the case in which the interference term in eq. (6), no longer corresponds to individual photons but to a conglomerate of photons, we have that the description of probability for the position of a photon, is now associated with the intensity, since it addresses the position for n

photons corresponding to diffraction pattern, light or dark areas, according to which it can be said that:

$$I_{AB} = I_{AB} - I_A - I_B \quad (7)$$

From the eq. (3), (5) and (7) can easily be deduced that:

$$I_{ABC} = |\psi_A(\vec{r}) + \psi_B(\vec{r}) + \psi_C(\vec{r})|^2 \quad (8)$$

It means,

$$I_{ABC} = |\psi_A|^2 + |\psi_B|^2 + |\psi_C|^2 + \psi_A^* \psi_B + \psi_B^* \psi_A + \psi_B^* \psi_C + \psi_C^* \psi_B + \psi_C^* \psi_A + \psi_A^* \psi_C \quad (9)$$

$$I_{ABC} = I_{AB} + I_{BC} + I_{CA} + I_{AB} + I_{BC} + I_{CA} \quad (10)$$

$$I_{ABC} = I_{AB} + I_{BC} + I_{CA} + (I_{AB} - I_A - I_B) + (I_{BC} - I_B - I_C) + (I_{CA} - I_C - I_A) \quad (11)$$

$$I_{ABC} = I_{AB} + I_{BC} + I_{CA} - I_A - I_B - I_C \quad (12)$$

Thus, if one considers eq. (12) together with the illustration of Fig. 3, it can be found that complete diffraction can be reconstructed from the relationship of intensity patterns of single and double apertures [14].

Using the label sets of Fig. 3, an OAM beam is diffracted as described in eq. (1), resulting in the diffraction patterns shown in Fig. 4, 5.

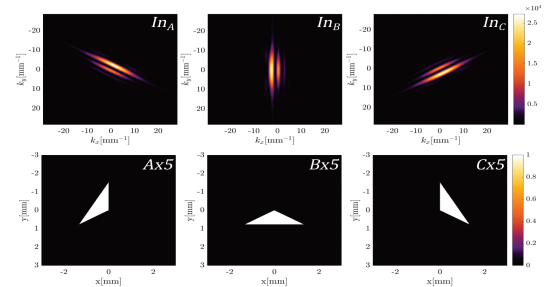


Figure 4. Diffraction patterns for $m = 3$, due to the contribution of each separate, disjoint and labeled slits as A, B, C. Source: The Authors.

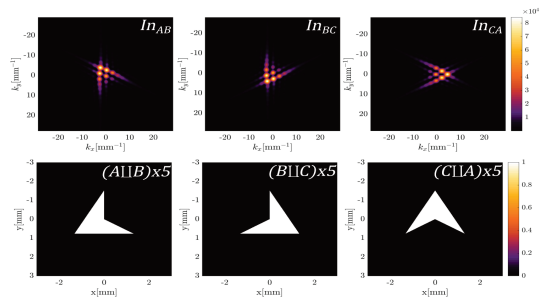


Figure 5. Diffraction patterns contributions due to each pair of independent slits labeled AB, BC and CA. Source: The Authors.

It is important to note that the individual slits constituting the complete triangular equilateral aperture; **A**, **B** and **C**, they never intercept. $x5$ represents an increase of five times, compared to the original image, for visualization purposes. Thus, by considering the combination in eq. (12), it is possible to recover the diffraction pattern associated with an OAM beam, as seen in Fig. 6.

With this brief discussion, the validity of Born's rule is verified numerically for an equilateral triangular aperture, providing a simple explanation of the array of bright spots that appear, which allows the determination of the magnitude and sign of the topological charge of OAM beam. Taking a lot of importance in the proposed decoder, since although changes occur in the diffraction pattern, information is preserved, only its representation is modified.

Now, a vortex is made to diffract on a straight edge of thick thickness e , such that $e \gg \lambda$, Located on the transversal symmetry axis of the mode. The triangular aperture is used as a tool to verify the information in the OAM field distribution that is diffracted. In Fig. 7, the diffraction pattern obtained from the numerical simulation is showed.

Although the pattern of spots is not present, the information of the vortex is preserved after diffraction by the thin straight edge. For this reason, if you look closely, the pattern of lines in Fig. 7. (c), maintains a symmetry by means of which it is possible to identify the sign and the topological charge value in the incident OAM beam, is an alternative manner.

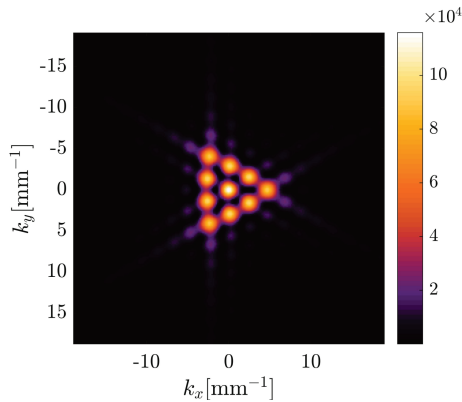


Figure 6. Reconstructed diffraction pattern for $m = 3$. Source: The Authors.

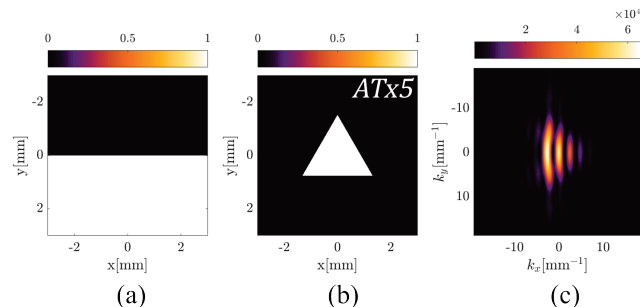


Figure 7. Diffraction pattern of an OAM beam with $m = 3$, by an straight edge (a), using an equilateral triangular aperture to evaluate the topological charge (b) and, the simulation results (c). Source: The Authors.

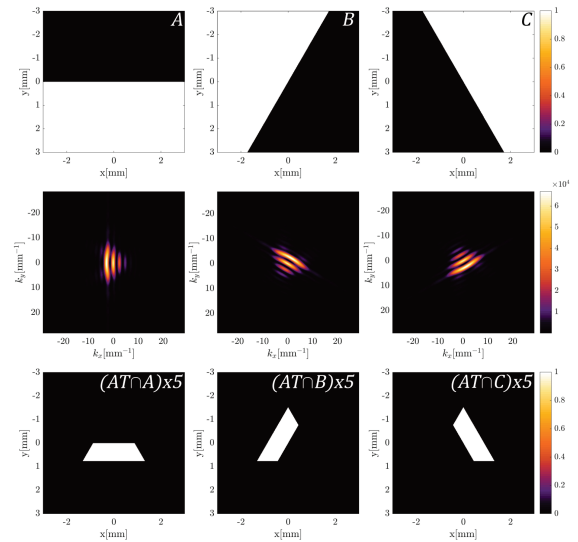


Figure 8. Diffraction patterns for an incident OAM beam with topological charge three diffracted by an edge (A, B or C) and its analysis using an equilateral triangular aperture AT. Source: The Authors.

A positive or negative slope of the edge orientation on the transversal plane to the optical axis allows patterns identical to those in Fig. 7. (c) to be obtained but rotated and in accordance with the inclination of the edge, as shown in Fig. 8.

In order to verify the conservation of the information on diffraction pattern, slits labeled as $AT \cap A$, $AT \cap B$, $AT \cap C$ correspond to the intersection between the triangular aperture AT and the straight edge in three different orientations (A, B and C) shown in first line. As already shown, it is possible to recover the diffraction pattern of an OAM beam by an equilateral triangular aperture, following the postulate of Born [15], from the relation between simple and mutually disjoint sets.

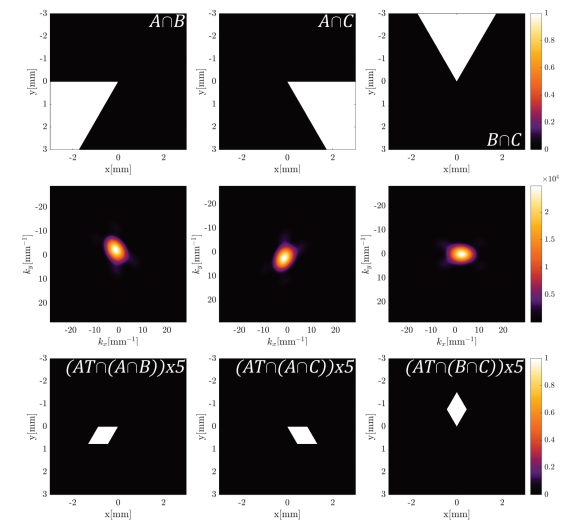


Figure 9. Diffraction pattern for an incident OAM beam with topological charge three diffracted by a double straight edge ($A \cap B$, $A \cap C$ or $B \cap C$) and its analysis using an equilateral triangular aperture AT. Source: The Authors.

The grooves of Fig. 8., are the result of studying the straight edge so that its orientation coincides with the orientation of the sides of equilateral triangle.

Now in Fig. 9. we study the intersection between the straight edges ($A \cap B$, $A \cap C$ and $B \cap C$), with the triangular aperture generating the slits $AT \cap (A \cap B)$, $AT \cap (A \cap C)$, $AT \cap (B \cap C)$.

From Fig. 10, the symmetry of the slits emulated by the superposition of different straight edge orientations and the triangular aperture, shows how these slits ($A \cap B$, $A \cap C$ and $B \cap C$) are not mutually disjoint, which implies that Born's rule [13], is not applicable.

Although the conditions for using the Born rule are not met, it is possible to construct the resulting field by adding the diffraction figures for the three mutually rotated edges viewed through the triangular aperture as shown in Fig. 11. (b), so that by operating these diffraction figures as described below, it is also possible to reconstruct the diffraction pattern of the propagating OAM beam.

$$I_{n_{Bordes\ ABC}} = I_{n_{AT \cap A}} + I_{n_{AT \cap B}} + I_{n_{AT \cap C}} \quad (13)$$

Where $I_{n_{AT \cap i}}$ is the intensity pattern due to edge i ($i = A, B, C$) viewed through the aperture AT .

Upon careful examination of Fig. 10. (b) it is possible to identify that the generated apertures ($AT \cap (A \cap B)$, $AT \cap (A \cap C)$, $AT \cap (B \cap C)$) are mutually disjoint and they're contained in slits of Fig. 10. (a) ($AT \cap A$, $AT \cap C$, $AT \cap B$). For that reason, eq. (13) contains the first three terms of the Born rule for three disjoint slits contained in the equilateral triangular aperture, where the first three terms of intensity correspond to the diffraction due to double slits [13].

If we complete the eq. (13) added with the interference terms due to the double straight edges, ($A \cap B$, $A \cap C$, $B \cap C$), the following is obtained:

$$I_{n_{Bordes\ ABC}} = I_{n_{AT \cap A}} + I_{n_{AT \cap B}} + I_{n_{AT \cap C}} - I_{n_{AT \cap (A \cap B)}} - I_{n_{AT \cap (B \cap C)}} - I_{n_{AT \cap (A \cap C)}} \quad (14)$$

Where I_{n_i} is the diffraction pattern due to the simple and double edges i ($i = A, B, C, A \cap B, A \cap C, B \cap C$) respectively viewed since the aperture AT . In Fig. 11. (c) is shown the addition obtained for the diffraction patterns of OAM beam.

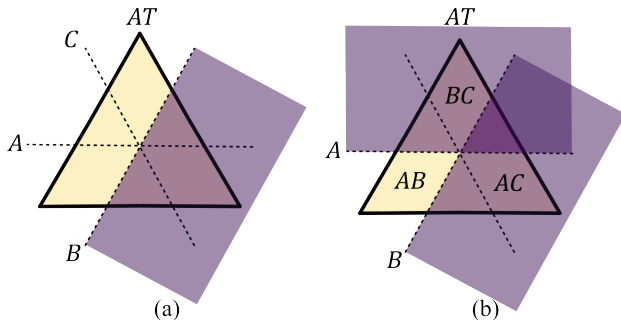


Figure 10. Interaction's geometry, straight edge – triangular equilateral aperture ($AB = A \cap B$, $AC = A \cap C$, $BC = B \cap C$).

Source: The Authors.

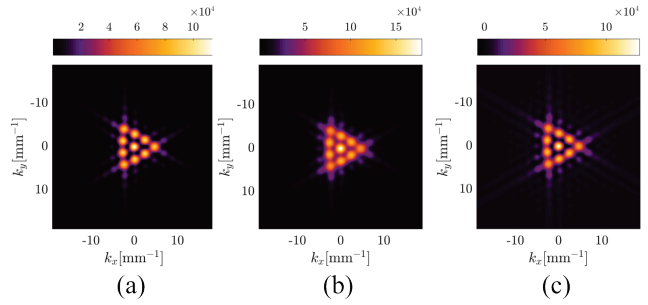


Figure 11. Theoretical diffraction pattern (a), reconstruction by the eq. (13) (b), reconstruction by the eq. (14) (c) for a OAM beam with topological charge three.

Source: The Authors.

Table 1.

Correlation between reconstructed and theory diffraction patterns.

	R1	R2
m=1	~0.9589	~0.9771
m=3	~0.9591	~0.9962
m=5	~0.9610	~0.9993
m=7	~0.9604	~0.9999
m=9	~0.9596	~1.0000

Source: The Authors.

As observed in Fig. 11. (b) and 11.(c), The addition of diffraction figures is more than sufficient to identify the topological charge of incident OAM beam [11], although the straight edges are not mutually disjoint.

Correlating images obtained in Fig. 11.(b) and images in Fig. 11.(c) with Fig. 11.(a), correlation factors of approximately 0.9591 and 0.9962 are obtained (See Table 1).

To verify the validity of the approximation in eq. (13) and (14), the reconstruction of the diffraction patterns corresponding to different upper and lower orders of topological charge value is performed. The above-mentioned correlations are calculated and shown in the Table 1.

The current analysis of this technique to calculate the topological charge of an OAM beam, has been reported to make possible the identification of optical vortices with topological charge of up to $m = 20$. That is to say, when used in combination with a rectangular aperture, the triangular aperture allows to identify the sign of the TC and, the rectangular aperture for even modes, provides an accurate description of the phase structure of the incident OAM beam by means of the number of external light spots [16]. Focusing on the triangular aperture and its interaction with a straight edge, it would be more efficient to count lines and, with a criterion of symmetry in addition to the counting of maxima, to identify topological charges with greater value.

In Fig. 12, dot pattern corresponding to $m = 20$ can be easily measured. Although respectively the correlation factors R1 and R2 are ~0.9487 and ~0.9999, the images are difficult to interpret. For this reason, a numerical simulation of an OAM beam with $m = 21$ diffracted by a straight edge seen through a triangular aperture (see Fig. 13. (a)) is conducted. In this way, we can overcome what has so far been achieved with triangular apertures, in identifying high TC for an incident OAM beam [16].

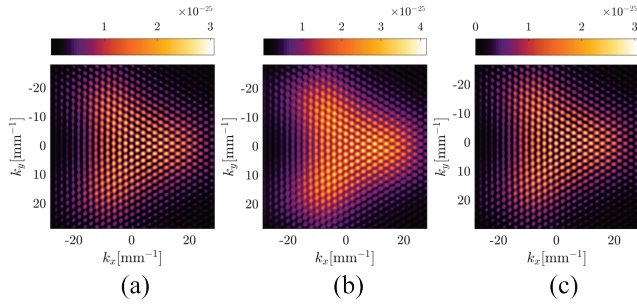


Figure 12. Theoretical diffraction pattern (a), reconstruction from eq. (13) (b), reconstruction from eq. (14) (c), for a beam with topological charge twenty. Source The Authors.

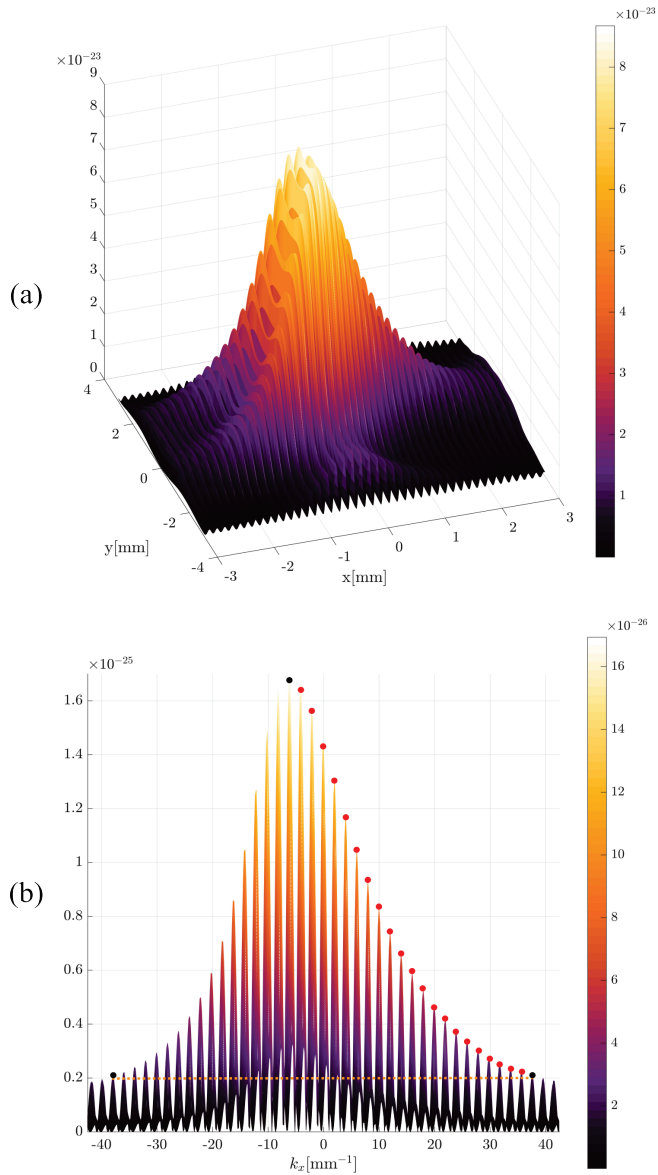


Figure 13. Diffraction figure of an incident OAM beam with topological charge twenty-one, by an edge, using an equilateral (upper) triangular aperture for its evaluation. Horizontal profile to the center of the diffraction plane (bottom). Source: The Authors.

If considered, a horizontal profile centered on the plane of diffraction pattern, gives a graph such as that of the Fig. 13. (b), which allows to identify in a simpler way, the topological charge, using the position of the global maximum and the number of maxima in the range of symmetry. This represents a simple and valuable processing at the time of its implementation. Thus, symmetry error is calculated to verify the effectiveness of the method for azimuthal phase factors greater than 20, obtaining 1.69% error among the coincident maxima.

The decoding system based on the maximum count was validated experimentally and numerically. To perform the latter, a model is proposed, which describes, through parameters of transmittance, thickness and index of refraction, the influence of the straight edge of nanometric film on a vortex with orbital angular momentum.

As shown in Fig. 14., the geometry of model proposed allows to introduce a multiplicative complex term to the OAM beam after diffraction by the straight edge. The refraction index of material (n_i), is normally associated with a delay in the propagation time of the electromagnetic wave, is a phase term. The phase introduced by the deposited film must maintain a proportional relationship between the total phase (2π) in one wavelength (λ), according to its thickness (d). From the transmitted intensity point of view, its transmittance (T_i) must be considered.

The relative position of the vortex with respect to the edge of the straight film is among the important features in the development of the model, assuming the vortex centered on the optical axis of propagation. It is important to note the transition between the substrate and the border of grown film, which implies a relationship between the individual transmittance of the two halves (See Fig. 14).

The pattern of lines on the far-field, resulting from the optical vortex-straight edge interaction seen with the help of AT, is analyzed through the profile in intensity of the image acquired and viewed by computer using a CCD camera. This profile shows variable horizontal dissymmetry, depending of the relative position of the edge with regards to the optical axis. Because of this, a micrometric scanning was performed,

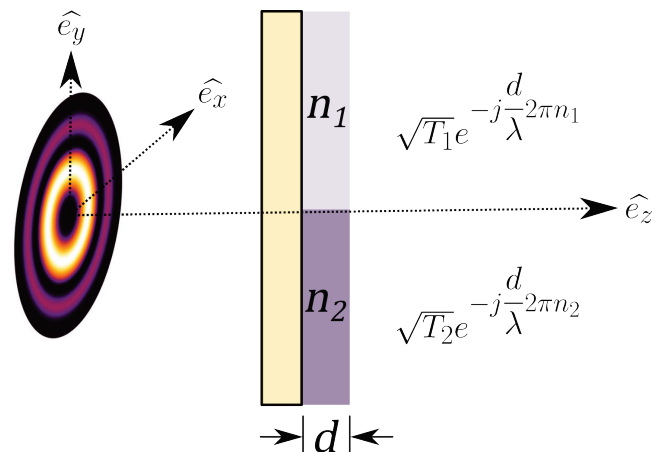


Figure 14. Geometry proposed for a straight edge obstacle of longitudinal dimension comparable to the incident wavelength of OAM beam. Source: The Authors.

retaining five vertical positions of the film border (see Fig.15.). From the analysis of these profiles, an identification rule based on the maximum counts, referred to the absolute maximum and between symmetrical lateral peaks is proposed.

Numerically, diffraction in the far field of an OAM beam with $m = 3$ is obtained by focusing on the edge, for different vertical positions relative to the optical axis of propagation, as seen in Fig. 16.

A profile is drawn for three different patterns as shown in Fig. 17., where the existing dissymmetry is confirmed. The symmetry error is evaluated between lateral maximums that appear to be symmetrical, for the five edge positions (tagged as $\bar{x}_1, \bar{x}_2, \bar{x}_3, \bar{x}_4, \bar{x}_5$) and it is shown in Table 2. With this criterion, the profiles of \bar{x}_2 and \bar{x}_4 , are contrasted, so that when viewing the position of the global maximum with respect to the center of the frame, it is possible to identify the sign of the topological charge, easily and effectively in the profile \bar{x}_4 .

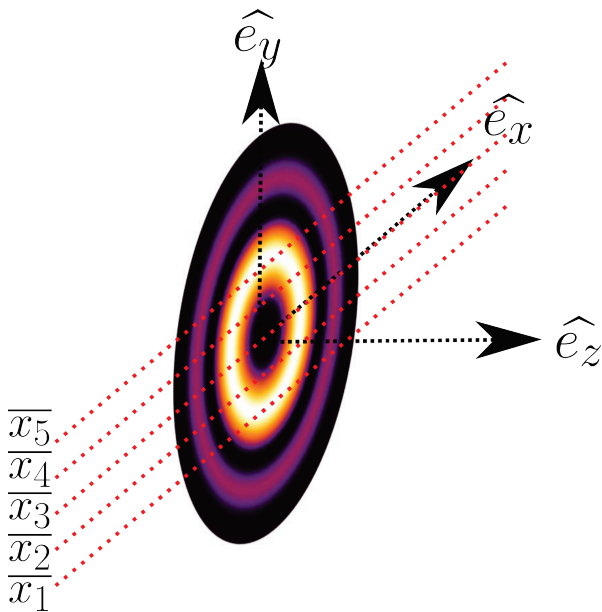


Figure 15. Vertical successive relative positions of the nanometric straight edge used. The rings represent the OAM incident beam relative to border position.
Source: The Authors.

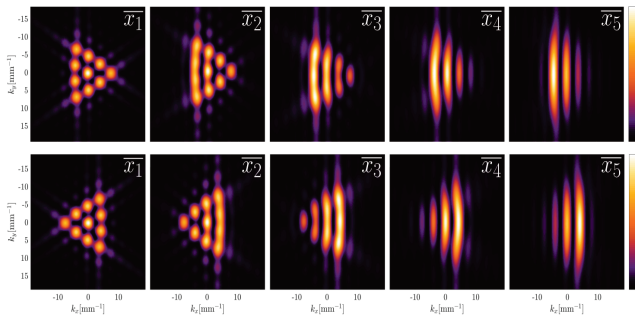


Figure 16. Diffraction figures associated with topological charges, $m = \pm 3$ for five vertical positions relative to the optical vortex of incident OAM beam.
Source: The Authors.

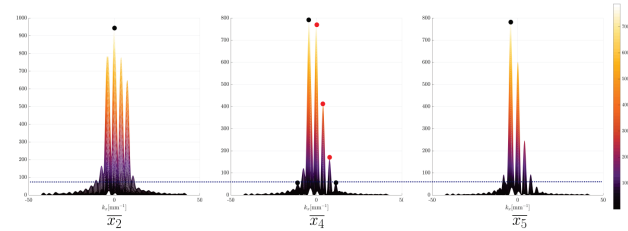


Figure 17. Intensity horizontal profiles for the diffraction patterns associated to the interaction of the OAM beam with topological charge $m=+3$. Diffraction is produced by a straight edge nanometric size for three different vertical positions, seen through the triangular aperture AT and to the center of each diffraction pattern.
Source: The Authors.

Considering the measures of the right and left relative maximum with respect to the axis of symmetry of the plotted profile, one has:

Table 2. Quantified symmetry error between the first coincident lateral lobes, with respect to the profile center of diffraction pattern for $m = +3$.

	Left maximum	Right maximum	Simmtry Error
\bar{x}_1	321,6	102,60	68,65%
\bar{x}_2	977,7	966,6	1,13%
\bar{x}_3	1179,0	1239,0	4,8%
\bar{x}_4	1208,0	1178,0	2,48%
\bar{x}_5	865,0	773,3	10,60%

Source: The Authors.

Numerical diffraction of OAM beams with TC from $m = \pm 1$ to $m = \pm 5$, are shown in Fig. 18. The experimental implementation was performed with the device outlined in Fig. 19. by obtaining the far-field diffraction patterns shown in Fig. 22.

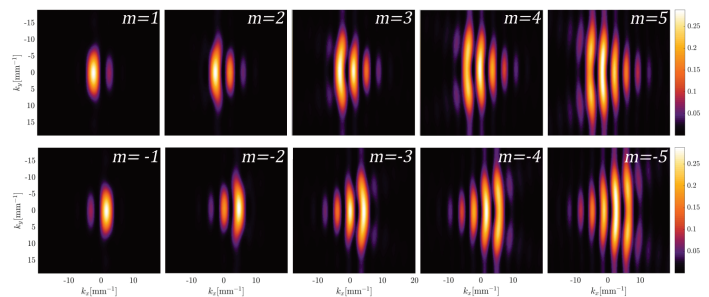


Figure 18. Simulated far-field diffraction of an OAM beam, $m = \pm 1 \rightarrow \pm 5$. Diffraction obtained by a straight edge of thick film, $e \gg \lambda$ seen through AT.
Source: The Authors.

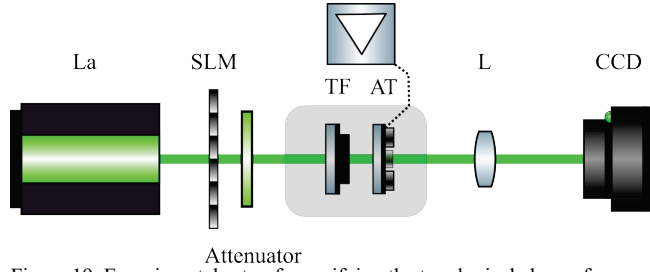


Figure 19. Experimental setup for verifying the topological charge from an OAM beam diffracted through straight edge.
Source: The Authors.

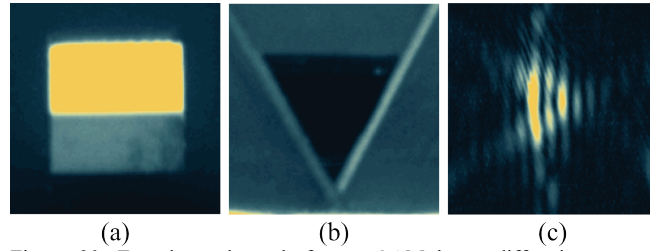


Figure 20. Experimental result for an OAM beam diffraction pattern (Topological charge is $m = +3$). Diffraction is produced by a straight edge of thickness ≈ 660 [nm] (a). Equilateral triangular aperture used to obtain the topological charge of the OAM beam (b) and, obtained pattern c).
Source: The Authors.

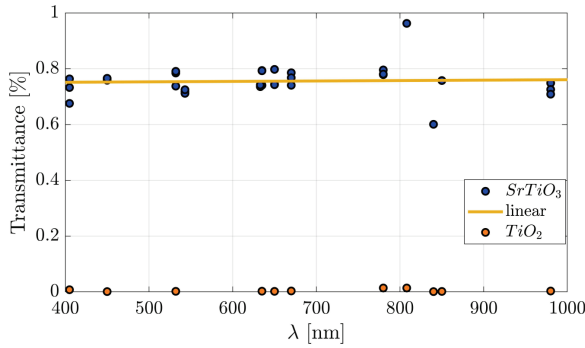


Figure 21. Experimental Transmittance curve for $SrTiO_3$ (Blue), and TiO_2 (Orange).
Source: The Authors.

3. Experimental results

The experimental setup done is shown in the Fig. 19.

Figure 19 shows: laser (La), Spatial Light Modulator (SLM), attenuator to control the energy of the OAM beam, thin film (TF), triangular equilateral aperture (AT), Fourier Lens (L) and CCD camera. In Fig. 20. (c) the numerical results of Fig 7. (c) are verified.

From the Fig. 20. when an OAM beam is diffracted by a nanoscale straight edge, centered at the optical propagation axis and seen through AT, a characteristic lines pattern is produced, which provides a good alternative for finding the magnitude and sign of the topological charge of the OAM beam at the time of its incidence. For simulation purposes,

this is achieved from transparent and dark areas (See Fig. 7.). Experimentally, nanoscale films with near-zero transmittance (TiO_2) and a thickness comparable to the wavelength, were grown on the middle of a substrate of $SrTiO_3$, whose transmittance in intensity is higher than 70%.

Next, the transmittance curves for the substrate and the film are measured for eleven wavelengths between 405 [nm] and 980 [nm]. The thickness of the films here is 660 [nm].

When the horizontally centered profiles are calculated for theoretical and experimental patterns as shown in Fig. 23., the symmetry measurements easily are obtained in Tables 3. and 4. After verifying the perfect concordance between the profiles obtained by numerical simulation and those obtained experimentally, it is the calculation of dissymmetry that allow to propose a new rule of measurement of TC:

$$CT = N_{m_i} - 1; \quad m_i > \gamma \pm \beta; \quad (15)$$

Where N_{m_i} represents the number of maxima, which satisfy the condition for m_i , greater than the threshold γ with a tolerance β (threshold of symmetry). The threshold is calculated, from the first coincident maximums after the global maximum, for which an estimate of the symmetry is made by measuring approximately coincident or closely coincident amplitudes. The tolerance allows that when they are not exactly coincident the symmetry parameter can be found.

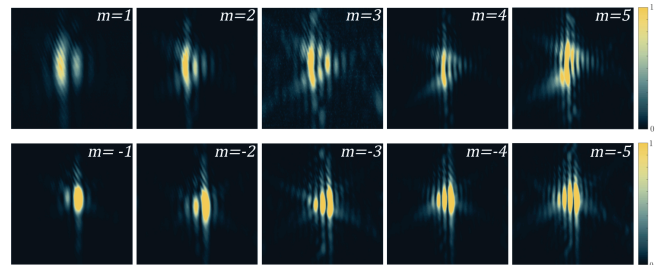


Figure 22. Experimental results of the far-field of different OAM beams, $m = \pm 1 \rightarrow \pm 5$, diffracted by the edge of $Ti = 0,2\%$, $e \approx 660$ [nm] film; view through AT.
Source: The Authors.

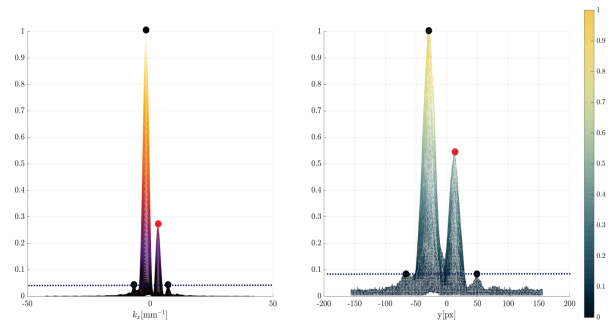


Figure 23. Intensity profiles in far-field for an OAM beam with CT $m = +1$ theoretical (left), experimental (right).
Source: The Authors.

Table 3.

Symmetry error between the first coincident lobes around the center of profile, for the diffraction pattern of an OAM beam with topological charge $m = +1 \rightarrow +5$, obtained by simulation.

	Left maximum	Right maximum	Simmtry error
$m = 1$	3966	3650	7.96%
$m = 2$	1887	1824	3.33%
$m = 3$	1208	1178	2.48%
$m = 4$	414.3	394.6	4.75%
$m = 5$	239.2	271.1	13.33%

Source: The Authors.

Table 4.

Symmetry error between the first coincident lobes around the center of profile, for the diffraction pattern of an OAM beam with topological charge $m = +1 \rightarrow +5$, experimentally obtained.

	Left maximum	Right maximum	Simmtry error
$m = 1$	22	21	4.5%
$m = 2$	21	25	19.04%
$m = 3$	37	42	13.51%
$m = 4$	16	15	6.25%
$m = 5$	18	27	5%

Source: The Authors.

From this result, is possible to appreciate the improvement introduced to techniques for detecting the topological charge of an OAM beam. Here is reduced to the diffraction of OAM beam by a straight edge and a triangular equilateral aperture analysis; due that the use of additional optics is suppressed which would be necessary for interferometric measurement and more efficient than optical vortex's radius measurement. In addition, this proposal decreases the cost of implementation. The rule described above in eq. (15) is essential to develop the algorithm capable of measure the information on the transmission channel of a data reception system. The system allows associate eight phase states to a combination of three bits. The eight states can be easily established e.g., from TC $m = \pm 1$ to ± 4 . This shows the advantage in increasing the channel capacity, since the transmission at the physical layer level is not given bit by bit.

4. Conclusions

The correspondence between the Fraunhofer diffraction patterns, obtained by simulation and those obtained experimentally for an incident OAM beam, was demonstrated when diffraction is produced by a straight edge of thick film ($>\lambda$) with a transmittance close to zero.

Born's rule was verified for classical conditions, which explains the formation of luminous bright spots net for the Fraunhofer pattern of an OAM beam diffracted by an equilateral triangular aperture. Additionally, a simple rule for the reconstruction of the diffraction pattern with slits that are not mutually disjoint is proposed. We find high correlation values when the reconstructed Fraunhofer pattern is correlated with respect to the original one.

Calculated values are more than 90%, which allow to identify in the reconstructed representations an appropriate correspondence for the measurement of the topological charge.

For incident OAM beams, which have diffracted through the straight edge of thick film and viewed through an equilateral triangular aperture it's possible to discriminate the value of its topological charge as well as its sign using the new rule proposed here. This proposed method eliminates the use of additional energy sources and optics, so that it is possible to efficiently identify the information contained in the optical vortex being propagated, since the identification of the sign is reduced to find the position of the global maximum with respect to the optical axis of propagation, and the magnitude to count of maxima that fall within the zone of symmetry, which is of vital importance in the implementation in a compact device.

Writing fork holograms on a SLM, the optoelectronic architecture for encoding and transmission of the information was generated, using as a channel the free space. In addition, including a nanometric film and a triangular equilateral aperture, the decoding architecture, which use the profile at center on diffraction pattern to identify the magnitude and sign of TC sending by the transmitter, was generated. Subsequently it was verified that the data sent corresponded to the received data, through the measurement made from eq. (15).

Acknowledgements

The authors thank Universidad Industrial de Santander – UIS, for supporting this research by means of the Research and Services Vice-chancellor (VIE), with funding project 1788: “Alternative description of total angular momentum, orbital and spin, in non-paraxial optics”. Additionally, they thank Colciencias for their support through the project: “Optics devices for quantum key distribution, high dimensionality system based in Orbital Angular Momentum of light” code 110256934957. The GOTS group, gives special thanks to professor Maria Elena Gómez de Prieto and Mario Fernando Quiñonez, from the thin films group of Universidad del Valle, for their invaluable help solving the problems found in the development of the project.

References

- [1] Cerecedo-Núñez, H.H. y Padilla-Sosa, P., Óptica y sus áreas de aplicación (una perspectiva general), Facultad de Física e Inteligencia Artificial, Universidad Veracruzana, México. [en línea]. [Consultado 20 de Julio de 2014]. Disponible en: <http://www.smf.mx/boletin/2005/Abr-05/Articulos-HCC.html>
- [2] Capilla, P., Artigas, J.M. y Pujol, J., Fundamentos de Colorimetría, Universidad de Valencia, España, Primera Edición, pp. 13- 183 (2002).
- [3] Allen, L., Beijersbergen, M., Spreeuw, R. and Woerdman, J., Orbital angular momentum of light and transformation of Laguerre-Gaussian laser modes, *Physical Review A*, 45 (11), pp. 8185-8189, 1992. DOI: 10.1103/PhysRevA.45.8185
- [4] 'Twisted light' carries 2.5 terabits of data per second, BBC. 25 de Junio de 2012 [en línea]. [Consultado: 21 de Julio de 14]. Disponible en: <http://www.bbc.com/news/science-environment-18551284>
- [5] Gibson, G., Courtail, J., Vasnetsov, M., Barnett, S., Franke, S., Padgett, A. and M., Increasing the data density of free-space optical

- communications using Orbital Angular Momentum, *Optics Express*, 12(22), pp. 54,4-5456, 2004. DOI: 10.1364/OPEX.12.005448
- [6] Wang, J., Yang, J.-Y., Fazal, I.M., Ahmed, N., Yan, Y., Huang, H., Ren, Y., Yue, Y., Dolinar, S., Tur, M. and Willner, A.E., Terabit free-space data transmission employing orbital angular momentum multiplexing, *Nature Photonics* 6, pp. 488-496, 2012. DOI: 10.1038/nphoton.2012.138
- [7] Díaz-Meza, C.F., Modelado de un sistema optoelectrónico para la codificación de información a través del momento angular orbital de la luz, Tesis Maestría en Ingeniería Electrónica, Facultad de Ingenierías Fisicomecánicas, Escuela de Ingeniería Eléctrica, Electrónica y Telecomunicaciones, Universidad Industrial de Santander, UIS, pp. 17-87, 2012.
- [8] Acevedo-Caceres, C.H., Análisis teórico – experimental de un haz con Momento Angular Orbital, Tesis Maestría en Física, Facultad de Ciencias, Escuela de Física Universidad Industrial de Santander-UIS, Colombia, 2012, pp. 56-79.
- [9] Stahl Ch. and Gbur, G., Analytic calculation of vortex diffraction by a triangular aperture, *J. Opt. Soc. Am. A.*, 33(6), pp. 1175-1180, 2016. DOI: 10.1364/JOSAA.33.001175
- [10] Hickmann, J.M., Fonseca, E.J.S., Soares, W.C. and Chávez-Cerda, S., Unveiling a truncated optical lattice associated with a triangular aperture using light's orbital angular momentum, *Phys. Rev. Lett.* 105(5), pp. 053904-1-053904-4, 2010. DOI: 10.1103/PhysRevLett.105.053904
- [11] Yongxin, L., Hua, T., Jixiong, P. and Baida, L., Detecting the topological charge of vortex beams using an annular triangle aperture, *Optics & Laser Technology*, 43, pp. 1233-1236, 2011. DOI: 10.1016/j.optlastec.2011.03.015
- [12] Sinha, U., Couteau, C., Jennewein, T., Laflamme, R. and Weihs, G., Ruling out multi-order interference in quantum mechanics, *Science*, 329(5990), pp. 418-421, 2010. DOI: 10.1126/science.1190545
- [13] Sorkin R.D., Quantum mechanics as quantum measure theory, *Mod. Phys. Lett. A.*, 9(33), pp. 3119-3127, 1994. DOI: /10.1142/S021773239400294X
- [14] Mesquita, P.H.F., Jesus-Silva A.J., Fonseca, E.J.S. and Hickmann, J.M., Engineering a square truncated lattice with light's orbital angular momentum, *Optics Express*, 19(21), pp. 20616-20621, 2011. DOI: 10.1364/OE.19.020616
- [15] Born, M., Zur Quantenmechanik der Stoßvorgänge, *Z. Phys.* 37(12), pp. 863-867, 1926. DOI: 10.1007/BF01397477
- [16] Silva, J.G., Jesus-Silva, A.J., Alencar, M.A.R.C., Hickmann, J.M. and Fonseca, E.J.S., Unveiling square and triangular optical lattices: a comparative study, *Optics Letters* 39(4), pp. 949-952, 2014. DOI: 10.1364/OL.39.000949
- J.H. Mendoza-Castro**, received his title as BSc. an Electronic Engineer by the Industrial University of Santander, Colombia in 2015. He currently is an Electronic Engineer master student working as a researcher in projects related to the applications of orbital angular momentum (OAM) of light in Quantum communications. He participated in a research stay on exploring OAM in stimulated Brillouin scattering processes at Nano Institute – The University of Sydney in 2018. ORCID: 0000-0002-2456-8771
- C.H. Acevedo**, received the BSc. title of Physicist by the Industrial University of Santander, Colombia in 2010. In August 2010, he joined the master's program in Physics at the same university and developed a research project on the theoretical and experimental part of luminous beams with orbital angular momentum, and obtained a MSc. in Physics in 2012. He participated in a research stay on angular momentum in electromagnetic fields at CREOL – Central University of Florida, USA in 2012. He received his Dr. in physics at the University Industrial de Santander, is member of the Group of Optics and Signal Processing, its research topic is related to the applications of orbital angular momentum in communications. Now, has a postdoctoral position at CREOL until end of this year. ORCID: 0000-0003-1700-6452
- C.F. Díaz**, received the BSc. in Electronic Engineer by the Industrial University of Santander, Colombia in 2008. In 2012, he obtained his MSc. in Electronic Engineering degree of the same University, developing an optoelectronic model for information coding with orbital angular momentum in a beam of light. He is currently researcher in a project related to the orbital angular momentum applications of light in photocatalysis. ORCID: 0000-0001-6882-0150
- Y. Torres**, is Dr. in Optics and Signal Processing at University of Franche-Comté, Besançon, France in 1983. He joined the Physics School of the Industrial University of Santander, Bucaramanga, Colombia in 1984, where he is professor of the School of Physics. He has done several postdoctoral stays at the Laboratoire d'Optique P.M. Duffieux, Besancon, France, Le Centre d'Optique, Photonique et Laser COPL, Québec, Canada, Laboratory of Image Processing, Terrasa, Spain, École Normale Supérieure de Télécommunications de Bretagne, Brest, France and Florida Atlantic University, Boca Raton, USA. His field of current interest, where he guides his research, is that of beams with orbital angular momentum and the applications of the Fourier Telescope technique. ORCID: 0000-0003-2507-2046
- J.G. Barrero**, received his BSc. in Electrical Engineer by the Industrial University of Santander, Colombia, in 1988. In 1995, he obtained a MSc. in Electronic Engineering from the same University. Its areas of activity are: electronic automation of electrical and industrial processes, signal processing and electronic process control. ORCID: 0000-0003-2443-8608